AGU PUBLICATIONS

Geophysical Research Letters

RESEARCH LETTER
10.1002/2016GL069529

Key Points:
- Diesel and biodiesel exhaust do not produce significant ice-nucleating particle concentrations
- Photochemical aging does not increase ice-nucleating particle concentrations in diesel exhaust
- Current parameterizations may overemphasize black carbon ice-nucleating particle concentrations globally

Supporting Information:
- Supporting Information S1

Correspondence to:
G. P. Schill,
gpschill@atmos.colostate.edu

Citation:
Schill, G. P., et al. (2016), Ice-nucleating particle emissions from photochemically aged diesel and biodiesel exhaust, *Geophys. Res. Lett.*, *43*, doi:10.1002/2016GL069529.

Received 9 MAY 2016
Accepted 14 MAY 2016
Accepted article online 18 MAY 2016

Ice-nucleating particle emissions from photochemically aged diesel and biodiesel exhaust

G. P. Schill[1], S. H. Jathar[2], J. K. Kodros[1], E. J. T. Levin[1], A. M. Galang[2], B. Friedman[3], M. F. Link[3], D. K. Farmer[3], J. R. Pierce[1], S. M. Kreidenweis[1], and P. J. DeMott[1]

[1]Department of Atmospheric Sciences, Colorado State University, Fort Collins, Colorado, USA, [2]Department of Mechanical Engineering, Colorado State University, Fort Collins, Colorado, USA, [3]Department of Chemistry, Colorado State University, Fort Collins, Colorado, USA

Abstract Immersion-mode ice-nucleating particle (INP) concentrations from an off-road diesel engine were measured using a continuous-flow diffusion chamber at −30°C. Both petrodiesel and biodiesel were utilized, and the exhaust was aged up to 1.5 photochemically equivalent days using an oxidative flow reactor. We found that aged and unaged diesel exhaust of both fuels is not likely to contribute to atmospheric INP concentrations at mixed-phase cloud conditions. To explore this further, a new limit-of-detection parameterization for ice nucleation on diesel exhaust was developed. Using a global-chemical transport model, potential black carbon INP (INP_{BC}) concentrations were determined using a current literature INP_{BC} parameterization and the limit-of-detection parameterization. Model outputs indicate that the current literature parameterization likely overemphasizes INP_{BC} concentrations, especially in the Northern Hemisphere. These results highlight the need to integrate new INP_{BC} parameterizations into global climate models as generalized INP_{BC} parameterizations are not valid for diesel exhaust.

1. Introduction

Ice-nucleating particles (INPs) are a rare subset of the atmospheric aerosol that affects the Earth's climate by modifying cloud cover, persistence, and brightness [*Vali et al.*, 2015]. Except in ice multiplication scenarios, ice-particle formation in the atmosphere at temperatures warmer than approximately −38°C can only be initiated by INPs. Despite their importance, the mechanisms surrounding atmospheric ice nucleation are complex and not well understood [*DeMott et al.*, 2011]; hence, there exist large uncertainties surrounding estimates of climate forcing from ice-containing clouds [*Boucher et al.*, 2013]. Several studies have implicated black carbon (BC) particles as possible INPs [e.g., *Twohy et al.*, 2010], as they represent a relatively abundant surface area for heterogeneous nucleation at altitudes relevant to mixed-phase clouds [*Schwarz et al.*, 2010a]. The role of BC as an INP, however, remains unclear. For example, field studies have shown that BC is enhanced in ice residuals sampled from mixed-phase clouds at Jungfraujoch [*Cozic et al.*, 2006, 2008], implicating the possible involvement of BC in ice nucleation; other studies at the same site, however, show opposite trends [*Kamphus et al.*, 2010]. Laboratory studies of ice nucleation on BC proxies exhibit similar conflicting results, with their effectiveness as INP ranging from below the limit of instrument detection to potentially rivaling the well-known INP mineral dust [*DeMott*, 1990; *Diehl and Mitra*, 1998; *Koehler et al.*, 2009; *Friedman et al.*, 2011; *Murray et al.*, 2012]. Despite this conflict, current global models that incorporate theoretical formulations of heterogeneous ice nucleation often identify BC as the second-most abundant INP type after mineral dust, with contributions ranging from 23% up to nearly 50% of all INP active [*Hoose et al.*, 2010; *Savre and Ekman*, 2015]. Certain types of biomass burning have been shown to be a source of BC INP (INP_{BC}) [*Petters et al.*, 2009; *Mccluskey et al.*, 2014] and have also been shown to impact ice formation in orographic clouds [*Twohy et al.*, 2010]; however, less is known about the contribution of INP_{BC} from fossil fuel sources. Additionally, atmospheric aging of BC after emission can alter its physicochemical properties [*China et al.*, 2015a]; therefore, it is reasonable to assume that aging may also alter its ice nucleation activity. Consequently, understanding BC as an INP, especially concerning specific sources and atmospheric aging, is essential to lowering the aforementioned uncertainty.

Here this uncertainty is directly addressed by measuring INP in the emissions of a real-world BC source, an off-road diesel engine. Emissions from diesel engines comprise approximately 20% of the global BC aerosol burden by mass, and the majority of BC emissions related to fossil fuel energy [*Bond et al.*, 2013]. Furthermore, diesel exhaust is a BC-rich source that has been identified as an effective target for mitigation of near-term climate forcing [*Bond et al.*, 2013]. Depending on the ice nucleation efficacy of diesel exhaust, however, mitigating BC

emissions from diesel exhaust may also alter cloud coverage through the so-called glaciation indirect aerosol effect [*Lohmann*, 2002]. In this study, emissions from combustion of both conventional and biodiesel fuels were explored, and the exhaust was photochemically aged for up to 1.5 equivalent days using an oxidative flow reactor. We show that neither fresh nor aged emissions from diesel engines contributed appreciably to atmospheric INP concentrations. To explore this, we developed a new limit-of-detection parameterization for diesel exhaust BC, and we estimated potential INP concentrations using a global-chemical transport model.

2. Experimental Setup

INP concentrations from diesel exhaust were measured using the Colorado State University continuous-flow diffusion chamber (CSU-CFDC) [*Rogers*, 1988; *Rogers et al*., 2001; *DeMott et al*., 2015]. Measurements were conducted during June 2015 in the Diesel Exhaust and Fuel + Controls (DEFCon) study at the CSU Powerhouse Facility's Engines Laboratory. A schematic of the experimental setup can be found in Figure S1 in the supporting information. In brief, the exhaust of a 4.5 L John Deere off-road diesel engine [*Drenth et al*., 2014] was sampled into a dilution chamber, which diluted the exhaust by a factor of 45–110; the engine meets the Tier 3 emissions standards set in 2007. Engine exhaust for both fuels was sampled under both idle conditions and 50% load (approximately 50% rated torque and 100% rated speed). For the ice nucleation experiments, neither a diesel particulate filter nor a diesel oxidation catalyst was employed downstream of the engine. The dilution chamber operates by aspirating room air that was filtered through a HEPA filter and a 208 L activated charcoal drum to scrub particles and volatile gases, respectively. The diluted exhaust was then passed through a potential aerosol mass (PAM) chamber [*Kang et al*., 2007]. The PAM chamber simulates photochemical aging by using an array of mercury lamps to photolyze H_2O to OH radicals; equivalent timescales of photochemical aging are determined from the OH radical concentration. Behind the PAM chamber, the flow was split to several particle measurement instruments, including the CSU-CFDC.

The CSU-CFDC samples an aerosol lamina between two vertically oriented concentric copper columns. The walls of the copper columns are chemically treated to be wettable by liquid water, which facilitates the formation of a thin, uniform layer of ice. The ice-coated walls are temperature controlled, which allows for specific control of the temperature and relative humidity (RH) in the aerosol lamina. For this study, the temperature and RH were set to approximately −30°C and 105% RH with respect to water, respectively. Over the course of all 151 experimental periods, the measured temperature and RH were -30.02 ± 0.12°C and 105.6 ± 0.4%, respectively; these experimental variabilities are lower than the typical instrumental uncertainties of ±0.5 K and 2.4% at −30°C [*DeMott et al*., 2015]. Under these water-supersaturated conditions, particles activate into droplets in the condensation/nucleation section, and those droplets which contain INP active at −30°C or warmer freeze. The lamina then enters an evaporation section held at ice saturation where droplets evaporate, but ice particles survive. Ice concentrations are determined from an optical particle counter (OPC) using a calibrated size threshold (i.e., 3.0 μm). The OPC also counts particles greater than 500 nm using a separate calibrated size threshold. A 2.4 μm impactor at the CFDC inlet was used to remove large particles to avoid miscounting them as ice crystals. The measured INP was corrected for background counts, and significance levels were determined as described in Text S1. All INP concentrations are reported at standard temperature and pressure.

Simultaneous measurements using a scanning mobility particle sizer (SMPS) and single-particle soot photometer (SP2) were also taken. For the SMPS, sizing scans were integrated to get the total number of particles between 32 and 829 nm. The SP2 used in this study has been described elsewhere [*Levin et al*., 2014]. In brief, optical detectors measure the interaction of individual aerosol particles with a high-intensity 1064 neodymium: yttrium/aluminum/garnet (Nd:YAG) laser. Those particles that absorb light at 1064 nm are heated to their vaporization temperature and emit thermal radiation, a process termed laser-induced incandescence. In the atmosphere these particles are primarily refractory BC (rBC), which can be verified using a dual color-band temperature measurement [*Schwarz et al*., 2006]. It is important to note that for this study, the SP2 had a lower limit of detection of 90 nm volume equivalent diameter, assuming a BC density of 2.0 g/cm^3 [*Schwarz et al*., 2010b]. Thus, BC number concentrations are reported only for particles containing BC cores between 90 and 500 nm.

3. INP Concentration Measurements

Figure 1 shows a time series taken from a typical experiment with the engine at 50% load. Total particle number concentrations and rBC number are shown in the bottom panel on the left and right axes, respectively. INP concentrations at 1 Hz are shown in the middle panel, and ~5 min time-averaged INP concentrations are shown in

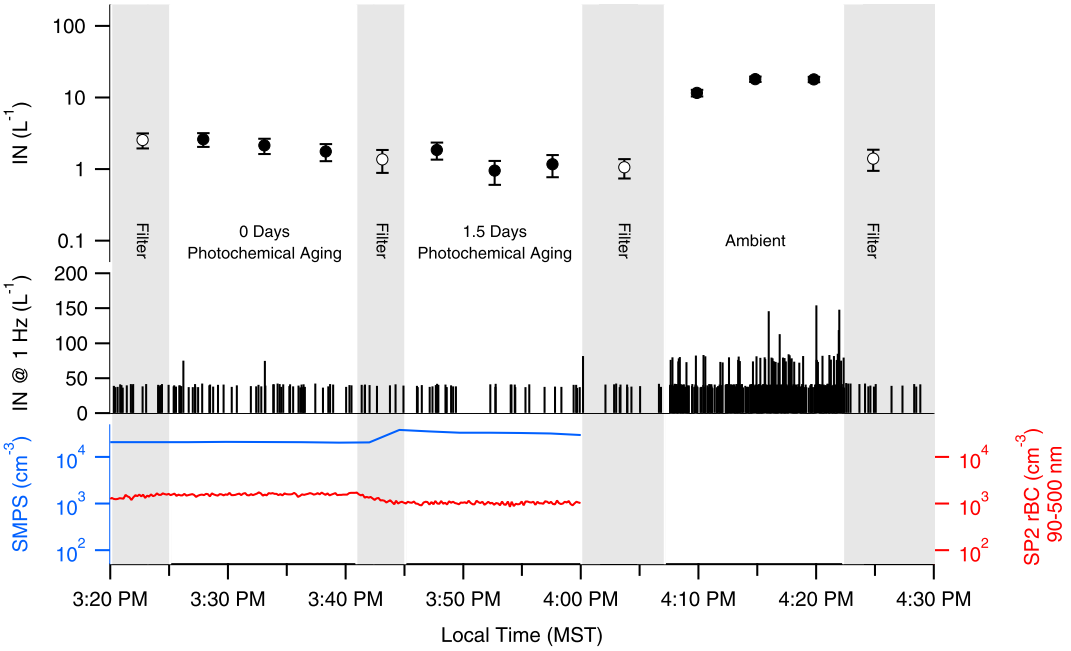

Figure 1. CSU-CFDC, SMPS, and SP2 data collected on 3 June 2015 for petrodiesel exhaust from an off-road diesel engine at 50% load that has been filtered, run through the PAM chamber with the lamps off (0 days aging), and aged 1.5 equivalent photochemical days in the PAM chamber. Also shown are CSU-CFDC data from ambient air in the CSU Powerhouse Facility's Engines Laboratory. The SMPS and SP2 data from the ambient air period are not available as these instruments were sampling diesel exhaust behind the PAM chamber.

the top panel. Filter-background periods for the CFDC are highlighted in grey. Typical background concentrations in this subset of experiments were ~2 L^{-1} (average of 1.1 L^{-1} for all 151 sampling periods). At 3:25 P.M., the CFDC inlet was switched from filter to sample. At this time, the aerosol concentration after the PAM chamber was ~20,000 cm^{-3}, and the number concentration of rBC-containing particles between 90 and 500 nm was greater than 1000 cm^{-3}. Despite high total particle and rBC number concentrations, the INP concentrations remained at ~2 L^{-1}, not significantly different than background level. Thus, the INP active fraction was less than ~1 in 10^7 of the total aerosol. After the second filter period, the voltage on the PAM chamber was set to 4 V; under normal circumstances, this corresponds to ~18 days photochemical aging, but significant OH radical suppression from organic species in the exhaust occurred in this study [*Link et al.*, 2016]. Thus, for this study, this setting corresponds to an OH exposure equivalent to 1.5 days of photochemical aging by OH at 1.5×10^6 molecules/cm^3. As shown, aging the exhaust to 1.5 photochemically equivalent days did not enhance the INP concentrations in diesel exhaust, which continued to be similar to the background. After the third filter period, the CFDC inlet was disconnected from the back of the PAM chamber and allowed to sample ambient room air in the CSU Powerhouse Facility's Engines Laboratory. Concentrations from the SMPS and SP2 are not shown because they were still sampling from the PAM chamber exit, but aerosol concentrations were much lower in the room air than in the exhaust. Despite this, the concentration of INP in the ambient air was approximately 10 L^{-1}, which is well above the background and agrees well with the *DeMott et al.* [2010] "global" INP parameterization.

Similar experiments on diesel and biodiesel exhaust were conducted for a total of 151 sampling periods. To facilitate a quantitative analysis between this work and previous studies, we use a modified version of the ice nucleation efficiency parameter ξ_T, as defined by *Petters et al.* [2009]:

$$\xi_T = \log_{10}(AF_{105}), \quad (1)$$

where AF_{105} is the fraction of all particles active as INP at ~105% RH. This parameter is slightly modified from the work of *Petters et al.* [2009], who used the maximum activated fraction by conducting supersaturation scans for each of their sampling periods and then used the activated fraction at the RH just prior to droplet breakthrough. As shown in the supporting information, our maximum activated fractions were not significantly different than those at 105% RH. The results for diesel emissions from all sampling periods are shown

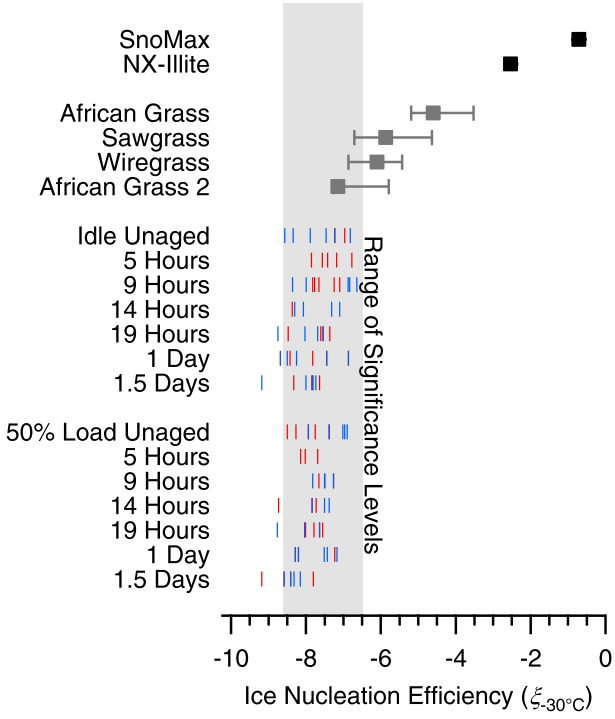

Figure 2. Ice nucleation efficiency of diesel (red sticks) and biodiesel (blue sticks) exhaust under idle and 50% load conditions. Also shown are time-averaged data for laboratory burns of biomass fuels from FLAME4 [*Levin et al.*, 2016] (dark grey markers) and from 500 nm size-selected SnoMax and NX-illite particles (this study; black markers). The range of significance for all diesel-exhaust sampling periods is highlighted in grey.

in Figure 2. For comparison, we show in Figure 2 ξ_{-30} determined for the emissions from the combustion of biomass fuels during the fourth Fire Laboratory at Missoula Experiment (FLAME4) [*Levin et al.*, 2016]. Figure 2 also includes data from this study for two proxies of mineral dust and ice nucleation active bacteria, NX-Illite and SnoMax, respectively. Each of these samples was size selected to 500 nm using a differential mobility analyzer.

From Figure 2, the range of calculated significance limits (highlighted in grey) for ξ_{-30} for all diesel experiments was between −6.5 and −8.6. This range of significance for ξ_{-30} depends on both the absolute significance levels (Text S1) and the total particle concentration. For the 151 time-averaged sampling periods, the total particle concentration varied from ~3000 cm^3 to 180,000 cm^3. Of these, the majority ($n = 148$) were under 90,000 cm^{-3}. Above 90,000 cm^{-3} and at $T = -30°C$, the vapor flux from the warm to the cold wall may not be sufficient to maintain the intended supersaturation leading to reductions >3% [*Levin et al.*, 2016]. Such conditions have been shown to result in systematic undercounting of INP activated fractions by 1 order of magnitude. Since our counts were below the significance level in all cases, it is impossible to correct for this potential undercounting. We note, however, that INPs were not shown to significantly increase during the supersaturation scans done in this study (Text S2). This suggests that undercounting due to reductions in the RH below 105% was likely minimal. All of the individual sampling periods for aged and unaged diesel and biodiesel under both idle conditions and 50% load in Figure 2 are below their individual significance level. Thus, no more than ~1 in 5×10^6 to 5×10^8 diesel exhaust particles will act as INP. This fraction is well below the fraction of INP in ambient aerosol in the free troposphere, as measured in previous studies [*Rogers et al.*, 1998]. Consequently, it is not likely that aged or unaged diesel and biodiesel exhaust will contribute significantly to atmospheric INP concentrations. In contrast, Figure 2 indicates that emissions from laboratory burns of some biomass fuels can produce ξ_{-30} above our range of significance. Thus, biomass burning may be a more important source of INP depending on the fuel type. Finally, all of the combustion particles are much less efficient than the laboratory proxies for mineral dust and ice-active proteins.

Although we did not investigate the temperature dependence of ξ_T, it is likely that INP concentrations decrease with increasing temperature, similar to previous field observations [*DeMott et al.*, 2010]. Thus, our measured ξ_{-30} are expected to be near the upper limit of the fraction of diesel-exhaust INP active as condensation/immersion-freezing nuclei under mixed-phase cloud conditions.

4. Limit-of-Detection Parameterization for Diesel-Derived INPs

Since ξ_{-30} from diesel and biodiesel exhaust are lower than our experimental significance levels, we can use our results to bound the maximum contributions to potential INP concentrations from these sources. To explore this further, we developed a new limit-of-detection (LOD) parameterization for BC particles

associated with diesel and biodiesel exhaust. Data from this experiment were evaluated under the singular hypothesis, which stipulates that the time dependence of freezing events is of secondary importance to the temperature dependence. In this vein, the data were parameterized using the ice nucleation active site density (n_s) model:

$$n_s(T) = -\frac{\ln([1 - \mathrm{AF}(T)]}{\mathrm{SA}_{\mathrm{aerosol}}}, \quad (2)$$

where AF is the fraction of INP in the total aerosol and $\mathrm{SA}_{\mathrm{aerosol}}$ is the surface area per particle. In order to ensure that we are representing the upper limit of n_s for BC in diesel exhaust, the following measures were taken. First, AF was estimated using the significance level for each of the individual sampling periods; these correspond to the highest possible INP concentrations that could have been present in diesel exhaust in these experiments without our detection. Further, we determined AF based not on the total number concentrations of particles, but rather using only the BC particle number concentrations derived from the SP2. The SP2 has a lower size limit of 90 nm volume equivalent diameter (VED), thus, we calculated the AF using the number concentrations of BC between 90 and 500 nm despite the majority of particles estimated to be smaller than 90 nm (Figure S3). Since 90 nm was the most abundant size measured by the SP2 (Figure S3), we estimated $\mathrm{SA}_{\mathrm{aerosol}}$ by multiplying the mass of a 90 nm VED rBC particle (~0.7 fg) by its Brunauer-Emmett-Teller surface area, which we assumed to be 108 m^2/g [*NIST SRM 1650b*, 2013].

The n_s calculated for BC from diesel and biodiesel exhaust aged up to 1.5 photochemically equivalent days was $8.09 \times 10^2\ \mathrm{cm}^{-2}$ at −30°C. This value is over 4 orders of magnitude smaller than the value of $3.11 \times 10^7\ \mathrm{cm}^{-2}$, which was derived from past studies of soot acting as INPs [*Murray et al*., 2012]. Since our data were taken at one temperature (−30°C), we extend our parameterization to temperatures as warm as −18°C by assuming that it has the same temperature bounds and follows the same functional form as the equation in *Murray et al*. [2012] (from here on referred to as M12) for soot. The full LOD n_s equation can be found in the supporting information (equation (S1)).

5. GEOS-Chem Model Study

To quantify the effect of this LOD parameterization on modeled $\mathrm{INP}_{\mathrm{BC}}$ concentrations, global maps of BC concentrations by source (i.e., fossil fuel and biomass burning) were first produced. To calculate BC concentrations, we used the Goddard Earth Observing System chemical-transport model (GEOS-Chem) version 10.01. Our simulations were driven by GEOS-5 assimilated meteorology fields (http://gmao.gsfc.nasa.gov) and included aerosol tracers for sulfate, sea salt, nitrate, ammonium, dust, organic carbon, and black carbon as well as 52 gas-phase species. We simulated the year 2010 with one month of model spin-up (not included in analysis) at $4° \times 5°$ horizontal resolution and 47 vertical layers. Black and organic carbon emissions from fossil fuel and biofuel combustion are from *Bond et al*. [2007] and biomass burning from the Global Fire Emissions Database version 3 (GFED3) [*van der Werf et al*., 2010]. In order to determine atmospheric BC concentrations by source, we ran two simulations: one simulation included all BC emission sources and one simulation included only biofuel and biomass-burning BC emissions (fossil fuel emissions off). Comparing these two simulations allowed us to isolate the BC from fossil fuel sources. To determine particle surface area, we applied the BET surface area, 108 m^2/g to the BC mass distributions. In order to get particle number, we scale modeled BC mass into size distributions assuming a lognormal distribution with number median diameter of 180 nm and a standard deviation of 1.8 (similar to *Karydis et al*. [2012]). Both fossil fuel and biomass-burning BC number concentration global maps at the surface and the annually and zonally averaged latitude versus pressure plots of BC number concentrations can be found in Figure S4.

To determine the global distribution of $\mathrm{INP}_{\mathrm{BC}}$ that would be predicted using existing parameterizations that are not specific to the source of BC, we applied the M12 soot INP parameterization to modeled fossil fuel and biomass-burning concentrations. Figure 3a shows the number concentrations of BC active as INP at −20°C ($[\mathrm{INP}_{\mathrm{BC}}]_{-20}$) at the surface in the model. The model predicted the highest annually averaged concentrations of $[\mathrm{INP}_{\mathrm{BC}}]_{-20}$ in the Northern Hemisphere high latitudes and over areas of regular biomass-burning events. In Figure 3b, we applied the LOD n_s parameterization for diesel exhaust to all fossil fuel sources, while applying the M12 parameterization to the BC from the nonfossil sources. Figure 3c shows the ratio of $[\mathrm{INP}_{\mathrm{BC}}]_{-20}$ in Figure 3b to that in Figure 3a. As indicated by a ratio near 1, there was essentially no reduction

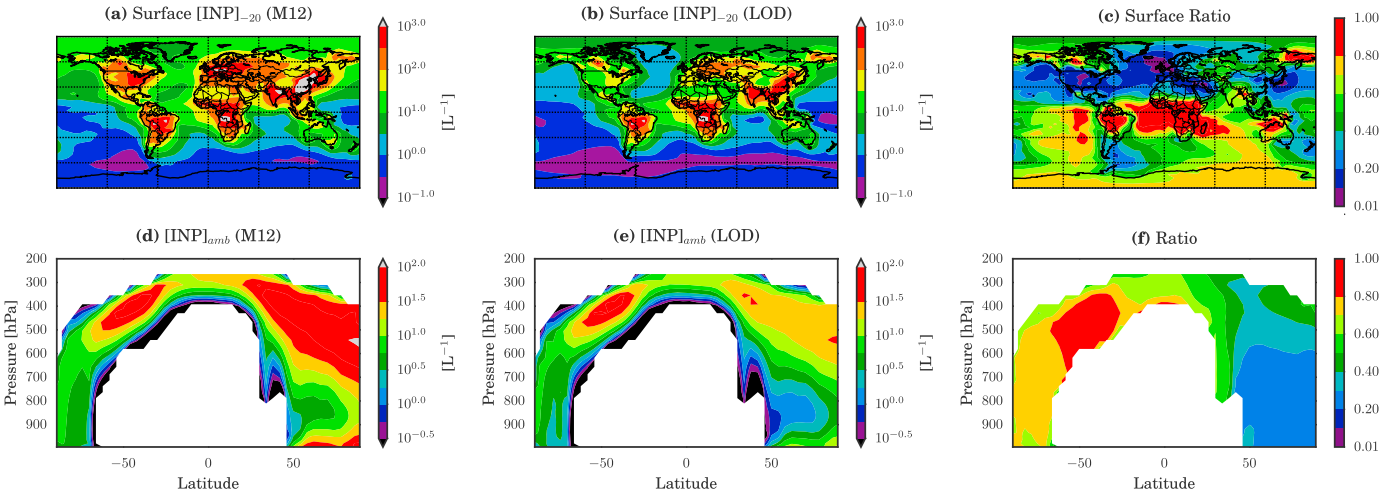

Figure 3. (a–c) Number concentrations of BC particles potentially active as immersion-freezing INP, as computed from GEOS-Chem aerosol fields. (Figure 3a) $[INP_{BC}]_{-20}$ at the surface using M12 parameterization for both fossil fuel and biomass-burning sources, (Figure 3b) $[INP_{BC}]_{-20}$ using M12 parameterization for biomass-burning sources and LOD parameterization for fossil fuel sources, (Figure 3c) ratio plot of b/a. (d–f) As in Figures 3a–3c, except that the number concentrations of black-carbon-derived INP are computed at the local temperatures, for temperatures $-38°C \leq T \leq -18°C$.

in $[INP_{BC}]_{-20}$ over sub-Saharan Africa and the Amazon basin, as BC emissions from these regions are largely from biomass burning, not fossil fuel sources. Likewise, the ratio plot shows values mainly >0.5 in the Southern Hemisphere. In the Northern Hemisphere, however, there are large changes in the concentrations of $[INP_{BC}]_{-20}$ at the surface, especially over areas of high industrial activity such as the United States, Europe, and China, where BC emissions are largely from fossil fuel sources. Thus, our LOD measurements of INP from diesel exhaust suggest that the current literature parameterization seems to be grossly overemphasizing INP_{BC} emissions in these areas.

In order to determine the concentrations from both types of sources of INP_{BC} that are transported to temperatures cold enough to form ice, we define the term $[INP_{BC}]_{amb}$ as the concentration of INP active at ambient temperatures derived from the model output. In other words, the parameterizations are evaluated based on local values of both BC concentrations and temperature. The annual zonal mean latitude versus pressure plots of $[INP_{BC}]_{amb}$ are shown in Figures 3d and 3e. It is important to note that the temperature bounds of both the M12 and LOD parameterizations are $-18°C$ and $-38°C$; outside of these temperatures, the parameterization goes to zero. Thus, this parameterization only accounts for those INP that would induce freezing in the immersion mode at temperatures relevant to mixed-phase clouds. Homogeneous freezing, occurring at temperatures colder than $-38°C$, is not parameterized. In Figure 3d, the M12 parameterization is applied to BC from both biomass burning and fossil fuel sources. In Figure 3e, the LOD parameterization is substituted for BC derived from fossil fuel emissions. Similar to $[INP_{BC}]_{-20}$ in the global distribution maps, there are large interhemispheric differences in $[INP_{BC}]_{amb}$. This difference is particularly striking in the Arctic regions, where the M12 parameterization may be overemphasizing $[INP_{BC}]_{amb}$ by a factor of 5, as shown by the ratio of Figure 3e over 3d (Figure 3f). This is due to the model attributing a large proportion of BC in this region to transported fossil fuel emissions, which we have shown to be an inefficient INP. Additionally, despite lower absolute concentrations and higher $[INP_{BC}]_{amb}$ ratios, the model shows that the M12 parameterization may overemphasize $[INP_{BC}]_{amb}$ in some regions of the Southern Hemisphere. Thus, Figure 3 suggests that applying a general parameterization to all BC, which appears to be invalid for diesel emissions, may overemphasize INP concentrations from BC, especially in Northern Hemisphere high latitudes.

6. Summary and Conclusion

Our laboratory measurements indicate that exhaust from diesel engines combusting either conventional or biodiesel fuels have ξ_{-30} values lower than approximately -6.5 to -8.6. These efficiencies, even when combined with the high number concentrations of emitted particles, are not high enough to contribute substantially to

atmospheric concentrations of immersion-mode ice-nucleating particles at mixed-phase cloud temperatures, even when aged up to 1.5 photochemically equivalent days. This finding is consistent with previous studies on diesel exhaust from on-road engines [*Chou et al*., 2013; *China et al*., 2015b]; however, those studies had a ξ_T lower limit of -3 and, therefore, could not fully characterize the limited atmospheric relevance of diesel exhaust INPs. Further, those studies did not investigate the effects of different fuel types and only probed aging timescales up to a few hours. Consistent with molecular dynamics studies [*Lupi and Molinero*, 2014], oxidative aging of the exhaust particles did not increase their ice nucleation efficiency in the immersion mode; however, some key atmospheric copollutants may have been missing in the PAM chamber. Our results also differ from the conclusions from laboratory studies on simple flame burner production of soot from acetylene and kerosene [*DeMott*, 1990; *Diehl and Mitra*, 1998], emphasizing the importance of measurements on real-world BC sources.

To explore the significance of these results, a LOD parameterization for BC, specific to diesel engine sources, was developed under the singular hypothesis. The predictions of ice nucleation active site densities from this parameterization are over 4 orders of magnitude lower than current parameterizations in the literature that were based primarily on laboratory studies of burner-soot particles. Both parameterizations were applied to global distributions of BC particle number concentrations that were modeled using GEOS-Chem, separating BC emissions into fossil fuel and biomass-burning sources. In contrast to our LOD n_s parameterization, using the current literature n_s parameterization for BC INPs from fossil fuel sources overemphasized INPs in the Northern Hemisphere, especially in the Arctic, a region of particular sensitivity to climate change due, in part, to the impact that cloud cover has on surface radiative fluxes [*Morrison et al*., 2011]. Furthermore, the persistence of these mixed-phase clouds is expected to be sensitive to INP concentrations [*Prenni et al*., 2007], as modest increases in ice concentrations can lead to the rapid conversion of mixed-phase clouds to all-ice clouds [*Morrison et al*., 2011]. Additionally, our findings could help explain INP biases in those global climate models that use theoretical representations of ice nucleation, which tend to overestimate ice nucleation from BC sources [*Savre and Ekman*, 2015]. Correcting these biases may be critical for correctly modeling future climate.

Finally, although we used the current literature parameterization for biomass-burning aerosol, BC from these sources may also be less efficient than INPs emitted from burner soot. Previous laboratory burns of various biomass fuels indicate that INP emissions from biomass burning are highly variable, both between burn types and burning conditions [*Petters et al*., 2009]; more recent laboratory burns confirm this behavior and can specifically attribute some ice nucleation behavior to rBC-containing particles [*Levin et al*., 2014]. Furthermore, *McCluskey et al*. [2014] have shown that certain biomass-burning events will emit and may even be dominated by a BC-type INP. Future studies should focus on further unraveling the physicochemical traits of BC-specific INP emissions from real-world biomass-burning events.

Acknowledgments

This material is based upon work supported by the National Science Foundation Division of Atmospheric and Geospace Sciences under award 1433517. Funding for E.J.T.L., S.M.K., P.J. D., and other logistical support was provided by NASA Earth Science Division award NNX12AH17G. Funding for B.F., M.F.L., and D.K.F. was provided through an Arnold and Mabel Beckman Young Investigator Award. Fees associated with the engine dynamometer tests (engine operation, equipment rental, fuel, and personnel) were supported by S.H.J. through startup funds as a new faculty hire at CSU. We would like to thank K. Evans for technical support and undergraduate researchers L. Lewane and N. Reed for test support during the campaign. G.P.S. thanks B. Palm for his assistance with the Carulite® O_3 scrubber. The data used are listed in the references, tables, supporting information, and in a digital repository at CSU (https://dspace.library.colostate.edu).

References

Bond, T. C., E. Bhardwaj, R. Dong, R. Jogani, S. Jung, C. Roden, D. G. Streets, and N. M. Trautmann (2007), Historical emissions of black and organic carbon aerosol from energy-related combustion, 1850–2000, *Global Biogeochem. Cycles*, *21*, GB2018, doi:10.1029/2006GB002840.

Bond, T. C., et al. (2013), Bounding the role of black carbon in the climate system: A scientific assessment, *J. Geophys. Res. Atmos.*, *118*, 5380–5552, doi:10.1002/jgrd.50171.

Boucher, O., et al. (2013), 7. Clouds and aerosols, *Clim. Chang. 2013 Phys. Sci. Basis. Contrib. Work. Gr. I to Fifth Assess. Rep. Intergov. Panel Clim. Chang.*, 571–657, doi:10.1017/CBO9781107415324.016.

China, S., et al. (2015a), Morphology and mixing state of aged soot particles at a remote marine free troposphere site: Implications for optical properties, *Geophys. Res. Lett.*, *42*, 1243–1250, doi:10.1002/2014GL062404.

China, S., et al. (2015b), Morphology of diesel soot residuals from supercooled water droplets and ice crystals: Implications for optical properties, *Environ. Res. Lett.*, *10*(11), 114010, doi:10.1088/1748-9326/10/11/114010.

Chou, C., Z. A. Kanji, O. Stetzer, T. Tritscher, R. Chirico, M. F. Heringa, E. Weingartner, A. S. H. Prévôt, U. Baltensperger, and U. Lohmann (2013), Effect of photochemical ageing on the ice nucleation properties of diesel and wood burning particles, *Atmos. Chem. Phys.*, *13*(2), 761–772, doi:10.5194/acp-13-761-2013.

Cozic, J., B. Verheggen, S. Mertes, P. Connolly, K. Bower, A. Petzold, U. Baltensperger, and E. Weingartner (2006), Scavenging of black carbon in mixed phase clouds at the high alpine site Jungfraujoch, *Atmos. Chem. Phys. Discuss.*, *6*, 11,877–11,912, doi:10.5194/acpd-6-11877-2006.

Cozic, J., S. Mertes, B. Verheggen, D. J. Cziczo, S. J. Gallavardin, S. Walter, U. Baltensperger, and E. Weingartner (2008), Black carbon enrichment in atmospheric ice particle residuals observed in lower tropospheric mixed phase clouds, *J. Geophys. Res.*, *113*, D15209, doi:10.1029/2007JD009266.

DeMott, P. J. (1990), An exploratory study of ice nucleation by soot aerosols, *J. Appl. Meteorol.*, *29*, 1072–1079, doi:10.1175/1520-0450(1990)029<1072:AESOIN>2.0.CO;2.

DeMott, P. J., A. J. Prenni, X. Liu, S. M. Kreidenweis, M. D. Petters, C. H. Twohy, M. S. Richardson, T. Eidhammer, and D. C. Rogers (2010), Predicting global atmospheric ice nuclei distributions and their impacts on climate, *Proc. Natl. Acad. Sci. U.S.A.*, *107*, 11,217–11,222, doi:10.1073/pnas.0910818107.

DeMott, P. J., et al. (2011), Resurgence in ice nuclei measurement research, *Bull. Am. Meteorol. Soc.*, *92*, 1623–1635, doi:10.1175/2011BAMS3119.1.
DeMott, P. J., et al. (2015), Integrating laboratory and field data to quantify the immersion freezing ice nucleation activity of mineral dust particles, *Atmos. Chem. Phys.*, *15*(1), 393–409, doi:10.5194/acp-15-393-2015.
Diehl, K., and S. K. Mitra (1998), A laboratory study of the effects of a kerosene-burner exhaust on ice nucleation and the evaporation rate of ice crystals, *Atmos. Environ.*, *32*(18), 3145–3151, doi:10.1016/S1352-2310(97)00467-6.
Drenth, A. C., D. B. Olsen, P. E. Cabot, and J. J. Johnson (2014), Compression ignition engine performance and emission evaluation of industrial oilseed biofuel feedstocks camelina, carinata, and pennycress across three fuel pathways, *Fuel*, *136*, 143–155, doi:10.1016/j.fuel.2014.07.048.
Friedman, B., G. Kulkarni, J. Beránek, A. Zelenyuk, J. A. Thornton, and D. J. Cziczo (2011), Ice nucleation and droplet formation by bare and coated soot particles, *J. Geophys. Res.*, *116*, D17203, doi:10.1029/2011JD015999.
Hoose, C., J. E. Kristjánsson, J.-P. Chen, and A. Hazra (2010), A classical-theory-based parameterization of heterogeneous ice nucleation by mineral dust, soot, and biological particles in a global climate model, *J. Atmos. Sci.*, *67*, 2483–2503, doi:10.1175/2010JAS3425.1.
Kamphus, M., M. Ettner-Mahl, T. Klimach, F. Drewnick, L. Keller, D. J. Cziczo, S. Mertes, S. Borrmann, and J. Curtius (2010), Chemical composition of ambient aerosol, ice residues and cloud droplet residues in mixed-phase clouds: Single particle analysis during the cloud and aerosol characterization experiment (CLACE 6), *Atmos. Chem. Phys.*, *10*, 8077–8095, doi:10.5194/acp-10-8077-2010.
Kang, E., M. J. Root, and W. H. Brune (2007), Introducing the concept of Potential Aerosol Mass (PAM), *Atmos. Chem. Phys. Discuss.*, *7*, 9925–9972, doi:10.5194/acpd-7-9925-2007.
Karydis, V. A., S. L. Capps, A. G. Russell, and A. Nenes (2012), Adjoint sensitivity of global cloud droplet number to aerosol and dynamical parameters, *Atmos. Chem. Phys.*, *12*, 9041–9055, doi:10.5194/acp-12-9041-2012.
Koehler, K. A., S. M. Kreidenweis, P. J. DeMott, M. D. Petters, A. J. Prenni, and C. M. Carrico (2009), Hygroscopicity and cloud droplet activation of mineral dust aerosol, *Geophys. Res. Lett.*, *36*, L08805, doi:10.1029/2009GL037348.
Levin, E. J. T., G. R. McMeeking, P. J. DeMott, C. S. McCluskey, C. E. Stockwell, R. J. Yokelson, and S. M. Kreidenweis (2014), A new method to determine the number concentrations of refractory black carbon ice nucleating particles, *Aerosol Sci. Technol.*, *48*(12), 1264–1275, doi:10.1080/02786826.2014.977843.
Levin, E. J. T., et al. (2016), Ice nucleating particle emissions from biomass combustion and the potential importance of soot aerosol, *J. Geophys. Res. Atmos.*, *121*, doi:10.1002/2016JD024879.
Link, M. F., B. Friedman, R. Fulgham, P. Brophy, A. Galang, S. H. Jathar, P. Veres, J. M. Roberts, and D. K. Farmer (2016), Photochemical processing of diesel fuel emissions form a large secondary source of isocyanic acid (HNCO), *Geophys. Res. Lett.*, *43*, 4033–4041, doi:10.1002/2016GL068207.
Lohmann, U. (2002), A glaciation indirect aerosol effect caused by soot aerosols, *Geophys. Res. Lett.*, *29*(4), 1052, doi:10.1029/2001GL014357.
Lupi, L., and V. Molinero (2014), Does hydrophilicity of carbon particles improve their ice nucleation ability?, *J. Phys. Chem. A*, *118*(35), 7330–7, doi:10.1021/jp4118375.
McCluskey, C. S., P. J. Demott, A. J. Prenni, E. J. T. Levin, G. R. Mcmeeking, A. P. Sullivan, T. C. J. Hill, S. Nakao, C. M. Carrico, and S. M. Kreidenweis (2014), Characteristics of atmospheric ice nucleating particles associated with biomass burning in the US: Prescribed burns and wildfires, *J. Geophys. Res. Atmos.*, *119*, 10,458–10,470, doi:10.1002/2014JD021980.
Morrison, H., G. de Boer, G. Feingold, J. Harrington, M. D. Shupe, and K. Sulia (2011), Resilience of persistent Arctic mixed-phase clouds, *Nat. Geosci.*, *5*, 11–17, doi:10.1038/ngeo1332.
Murray, B. J., D. O'Sullivan, J. D. Atkinson, and M. E. Webb (2012), Ice nucleation by particles immersed in supercooled cloud droplets, *Chem. Soc. Rev.*, *41*, 6519–54, doi:10.1039/c2cs35200a.
NIST SRM 1650b (2013), *Diesel Particulate Matter*, Natl. Inst. of Stand. and Technol., U.S. Dep. of Commer., Gaithersburg, Md.
Petters, M. D., et al. (2009), Ice nuclei emissions from biomass burning, *J. Geophys. Res.*, *114*, D07209, doi:10.1029/2008JD011532.
Prenni, A. J., P. J. DeMott, S. M. Kreidenweis, J. Y. Harrington, A. Avramov, J. Verlinde, M. Tjernström, C. N. Long, and P. Q. Olsson (2007), Can ice-nucleating aerosols affect Arctic seasonal climate?, *Bull. Am. Meteorol. Soc.*, *88*, 541–550, doi:10.1175/BAMS-88-4-541.
Rogers, D. C. (1988), Development of a continuous flow thermal gradient diffusion chamber for ice nucleation studies, *Atmos. Res.*, *22*(2), 149–181, doi:10.1016/0169-8095(88)90005-1.
Rogers, D. C., P. J. DeMott, S. M. Kreidenweis, and Y. Chen (1998), Measurements of ice nucleating aerosols during SUCCESS, *Geophys. Res. Lett.*, *25*(9), 1383, doi:10.1029/97GL03478.
Rogers, D. C., P. J. DeMott, S. M. Kreidenweis, and Y. Chen (2001), A continuous-flow diffusion chamber for airborne measurements of ice nuclei, *J. Atmos. Oceanic Technol.*, *18*(5), 725–741, doi:10.1175/1520-0426(2001)018<0725:ACFDCF>2.0.CO;2.
Savre, J., and A. M. L. Ekman (2015), A theory-based parameterization for heterogeneous ice nucleation and implications for the simulation of ice, *J. Geophys. Res. Atmos.*, *120*, 4937–4961, doi:10.1002/2014JD023000.
Schwarz, J. P., et al. (2006), Single-particle measurements of midlatitude black carbon and light-scattering aerosols from the boundary layer to the lower stratosphere, *J. Geophys. Res.*, *111*, D16207, doi:10.1029/2006JD007076.
Schwarz, J. P., J. R. Spackman, R. S. Gao, L. A. Watts, P. Stier, M. Schulz, S. M. Davis, S. C. Wofsy, and D. W. Fahey (2010a), Global-scale black carbon profiles observed in the remote atmosphere and compared to models, *Geophys. Res. Lett.*, *37*, L18812, doi:10.1029/2010GL044372.
Schwarz, J. P., et al. (2010b), The detection efficiency of the single particle soot photometer, *Aerosol Sci. Technol.*, *44*, 612–628, doi:10.1080/02786826.2010.481298.
Twohy, C. H., et al. (2010), Relationships of biomass-burning aerosols to ice in orographic wave clouds, *J. Atmos. Sci.*, *67*, 2437–2450, doi:10.1175/2010JAS3310.1.
Vali, G., P. J. Demott, O. Möhler, and T. F. Whale (2015), Technical note: A proposal for ice nucleation terminology, (February), *Atmos. Chem. Phys.*, 10,263–10,270, doi:10.5194/acp-15-10263-2015.
van der Werf, G. R., J. T. Randerson, L. Giglio, G. J. Collatz, M. Mu, P. S. Kasibhatla, D. C. Morton, R. S. DeFries, Y. Jin, and T. T. van Leeuwen (2010), Global fire emissions and the contribution of deforestation, savanna, forest, agricultural, and peat fires (1997–2009), *Atmos. Chem. Phys.*, *10*, 11,707–11,735, doi:10.5194/acp-10-11707-2010.